

Numerical Investigation of Thermal Behavior of CNC Machine Tool and Its Effects on Dimensional Accuracy of Machined Parts

Erick Matezo-Ngoma¹, Abderrazak El Ouafi¹, Ahmed Chebak²

¹Computer Science and Engineering Department, University of Quebec, Rimouski, Canada

²GTI, Mohammed VI Polytechnic University, Ben Guerir, Morocco

Email: Abderrazak_elouafi@uqar.ca

How to cite this paper: Matezo-Ngoma, E., El Ouafi, A. and Chebak, A. (2024) Numerical Investigation of Thermal Behavior of CNC Machine Tool and Its Effects on Dimensional Accuracy of Machined Parts. *Journal of Software Engineering and Applications*, 17, 617-637.
<https://doi.org/10.4236/jsea.2024.178034>

Received: June 6, 2024

Accepted: August 20, 2024

Published: August 23, 2024

Copyright © 2024 by author(s) and Scientific Research Publishing Inc. This work is licensed under the Creative Commons Attribution International License (CC BY 4.0).
<http://creativecommons.org/licenses/by/4.0/>



Open Access

Abstract

The dimensional accuracy of machined parts is strongly influenced by the thermal behavior of machine tools (MT). Minimizing this influence represents a key objective for any modern manufacturing industry. Thermally induced positioning error compensation remains the most effective and practical method in this context. However, the efficiency of the compensation process depends on the quality of the model used to predict the thermal errors. The model should consistently reflect the relationships between temperature distribution in the MT structure and thermally induced positioning errors. A judicious choice of the number and location of temperature sensitive points to represent heat distribution is a key factor for robust thermal error modeling. Therefore, in this paper, the temperature sensitive points are selected following a structured thermomechanical analysis carried out to evaluate the effects of various temperature gradients on MT structure deformation intensity. The MT thermal behavior is first modeled using finite element method and validated by various experimentally measured temperature fields using temperature sensors and thermal imaging. MT Thermal behavior validation shows a maximum error of less than 10% when comparing the numerical estimations with the experimental results even under changing operation conditions. The numerical model is used through several series of simulations carried out using varied working condition to explore possible relationships between temperature distribution and thermal deformation characteristics to select the most appropriate temperature sensitive points that will be considered for building an empirical prediction model for thermal errors as function of MT thermal state. Validation tests achieved using an artificial neural network based simplified model confirmed the efficiency of the proposed temperature sensitive points allowing the prediction of the thermally induced errors with an accuracy greater than 90%.

Keywords

CNC Machine Tool, Dimensional Accuracy, Thermal Errors, Error Modelling, Numerical Simulation, Finite Element Method, Artificial Neural Network, Error Compensation

1. Introduction

During machining operations, machine tools (MT) exhibit variant thermal behaviors due to thermal gradients generated by various internal and external heat sources. The irregular distribution of the temperature field in the MT structure produces thermal distortions which turn into thermal positioning error between part and tool, reducing the precision of the machined part. It is documented that thermally induced errors represent 40% to 70% of the total volumetric error [1]. Given their importance and impact on the dimensional accuracy of the machined parts, many researches have been conducted, in recent years, about MT thermal behavior analysis via simulations and experimentations and referring to thermal error estimation and prediction through analytical, numerical and empirical modeling approaches in order to produce an efficient thermal error compensation technology [2]-[9]. However, due to the variety of machining cycles, the change in cutting conditions from one machining operation to another, the use or not of cutting fluid and the evolution of environmental conditions, the thermal field is in constant variation [2], and it is very difficult to produce reliable models capable of accurately predicting thermally induced errors.

It is known that MT can be designed with symmetric structures and manufactured with materials possessing high thermal rigidity. Although most of these methods are effective in reducing thermal errors, they fail to entirely eliminate them and tend to increase manufacturing costs [3]. In contrast, thermal error compensation methods are much more practical and cost-effective, as they can be directly implemented without requiring expensive modifications to MT [10]. Nevertheless, it requires a reliable model capable of predicting errors in different MT operating conditions. A thermal error model consists of a mathematical formulation representing the relationships between position variations induced by thermal distortions of MT structure and temperature field characterized by temperature at carefully selected locations. This data is typically obtained using displacement sensors, laser interferometer, temperature sensors and thermal camera. During machining, thermal errors can be estimated using a thermal error model based on temperature data acquired in real time. Predicted error values are then used to adjust the MT positions in order to reduce machining errors [11]. The success of the entire compensation process largely depends on the accuracy of the thermal error model, which, in turn, relies on the number and the localization of the key temperature measurement points. The more precise the localization of temperature points on the machine, the more accurately the tem-

perature field can be captured. Too few key points may result in low prediction accuracy, while too many may adversely affect model robustness [12]. The selection of the appropriate group of temperature sensitive points is challenging due to the constantly evolving temperature fields influenced by various factors related to the MT, the process and the environment. As experiments are relatively expensive, numerical simulation remains an economical option for carrying out a thermos-elastic study to investigate the thermal behavior of the MT in order to characterize the most dominant heat distribution pattern through structured thermal mapping. This pattern can be used to identify the most relevant the most advantageous locations for temperature measurement.

2. Proposed Approach

The proposed approach consists of developing and experimentally validating a 3D numerical model to carry out a structured investigation and simulations of the MT thermomechanical behavior under thermal conditions representing as much as possible the real thermal conditions in MT normal operation in order to extract the possible relationships between temperature distributions and thermally induced distortions [13]. The proposed approach consists of following major steps:

- 1) Development of the 3D numerical model using finite element method.
- 2) Development of the experimental setup for temperature and thermal error measurements and experimentation for collecting the most useful data.
- 3) Validation of the numerical model.
- 4) Planning and execution of various series of simulations.
- 5) Data analysis and extraction of temperature sensitive points.
- 6) Selection of the predictive modelling technique and model establishment
- 7) Validation of the prediction model and compensation.

3. Numerical Modeling

Numerical modeling is carried out using FEM in order to characterize the behavior of MT structure under mechanical and thermal stresses [14]. The model consists in evaluating the temperature distribution as well as the resulting deformations based on non-linear thermal calculations, by discretizing the model of the MT structure into small elements solicited by sources of heat generation and heat exchanges (natural or forced convection, radiation, heat sources, etc.) [13]. The thermal deformation (ΔL_d) of the MT results from the combined effects of internal (ΔL_{in}) and external (ΔL_{ext}) heat sources as represented in Equation (1) along a given direction (X in this case).

$$\Delta L_d = \Delta L_{in} + \Delta L_{ext} \quad (1)$$

External heat sources affect the heat convection of the machine. When considering only the effect of environmental temperature, the MT structure deformation is assumed to be uniform and leads to linear thermal expansion [15].

$$\Delta L_{ext} = \alpha L_x (t_b(x_2) - t_b(x_1)) \quad (2)$$

where x_1 and x_2 are time points, $t_b(x_i)$ represents the transient temperature of the machine at time x_i . Excluding the source of internal heat, L_x is the nominal length and α is the coefficient of thermal expansion.

The MT structure exchanges heat with the surroundings based on Newton's cooling law, and the transient heat differential equation balance is expressed by Equation (3).

$$\frac{dt_b}{dx}(x) = \frac{1}{\tau_r} (t_b(x) - t_e(x)) \quad (3)$$

The temperature $t_b(x)$ at time x can be obtained in real-time, when the ambient temperature $t_e(x)$ at the time x , the time constant ($\tau_r = \rho c V / h A$) and the initial conditions are given [2].

3.1. Heat Generation and Thermal Source Analysis

The heat generation in the MT results from various thermal sources. It is a fact important in the study of the behavior of a machine. It results from the power of internal and external heat sources. This generation of heat is unavoidable in the deformation of the actual structure of the machine.

There are two thermal sources, external sources, and internal sources. Apart from the external thermal source, which is the temperature of the environment, we have the internal thermal sources of MT [16]:

- Heat generated between the ball nut and the axis ball screw shaft;
- Heat generated by the spindle and the support of the bearing of the ball screw due to the friction between the balls and the races;
- Heat generated by the rolling elements in the guides;
- Heat produced by the spindle motors and the drives;
- Heat generation by the axis motors of machine tools.

3.1.1. Heat Generation in Bearings

Most of the system's heat generation is caused by the machining process and friction between balls and bearings [17] [18]. However, in most cases, the heat of machining is reduced by coolant and fillings. Therefore, the friction between the balls and the bearings predominates in the rise in system temperature. The total friction torques in a bearing are measured with the loss of energy on the contact surfaces of the bearing components and the loss of energy caused by viscous friction [19]. The analytical estimation of frictional torque is overloaded with a multiplicity of factors, such as friction between rolling elements [20]. The frictional heat produced by the bearings is similar to that of the linear guide, which can be calculated by the following equation:

$$H_f = 1.047 \times 10^{-4} n \times M \quad (4)$$

where M is the frictional torque of the bearing, n is the rotational speed of the bearing and H_f is the power of the heat generated. The total friction torque M consists of two parts and can be calculated as follows:

$$M = M_1 + M_2 \quad (5)$$

where M_1 is the mechanical friction torque caused by the applied load and M_2 is the viscous friction torque caused by the viscosity of the lubricant.

$$M_1 = f_1 p_1 d_m \quad (6)$$

where f_1 is the bearing type and load factor, p_1 is the bearing preload, and d_m is the average bearing diameter. M_2 is calculated differently depending on whether the viscosity of cinematic lubricant is greater than, equal to, or less than 2000.

$$M_2 = 10^{-7} f_0 (v_0 n) \quad \text{if } v_0 n \geq 2000 \quad (7)$$

$$M_2 = 160 \times 10^{-7} f_0 d_m^3 \quad \text{if } v_0 n < 2000 \quad (8)$$

where f_0 is the bearing type and lubrication method factor and v_0 is the kinematic viscosity of the lubricant [17] [20].

3.1.2. Heat Generation on the Ball Screw Nut

The principle of heat generation on the ball screw nut is in general very similar to that of bearings. The heat is mainly generated by the friction between the balls and the grooves of the nut and between the balls and the grooves of the shaft. Nut load consists of two parts, *i.e.* preload and dynamic load [21]. The total frictional heat produced by the ball screw nut can be defined as [22]:

$$H_n = 0.12 \pi f_0 v_0 n T_n \quad (9)$$

where H_n is the total rate of frictional heat generated by the nut, f_0 is a factor related to the type of nut and the method of lubrication, v_0 is the kinematic viscosity of the lubricant, n is the rotational speed of the screw bearings, and T_n is the total frictional torque of the nut (the preload and the dynamic load).

3.1.3. Generation of Heat in the Linear Guide

The friction total heat produced in the linear guide results from the frictional force between rolling elements, rails, and carriages. Almost all friction losses in a bearing are transformed into heat inside the same bearing increasing its temperature. The total frictional heat in linear guide can be expressed by the heat rate (H_{gf}) [23].

$$H_{gf} = \eta F_{gf} V \quad (10)$$

where F_{gf} is the calculated frictional force in the linear guide, and V is the velocity. The friction force is a composition of coulomb friction force, viscous friction, and the strength of the Stribeck effect [24]. This frictional force is expressed by the following expression.

$$F_{gf} = (0.315 - 0.03 p_c) P \times 10^{-3} + \frac{1.52 p_c L_b}{v_i e^{-0.067(T-T_i)}} e^{0.015 \frac{-v}{v_i}} + L_b (0.003 L_b p_c V v_i e^{-0.067(T-T_i)} + 0.029) \quad (11)$$

where P is the external load, p_c is the preload class, and v is the kinematic viscosity. The frictional force is assumed to be completely converted into heat ($\eta = 1$) [19].

3.1.4. Heat Generation in the Spindle

The estimation of the thermal power of the bearings and the spindle motor is established in two parts. Bearing heat is generated in the contact areas. These areas exist due to friction between the balls and the external tracks [18]. Thus, the modeling of the H_{bf} thermal energy of the front and rear bearings of the spindle is determined by Equation (16).

$$H_{bf} = \frac{2\pi n}{60} T_b \quad (12)$$

The total heat generated from the motor H_m expressed in Equation (13) is mainly attributed to the loss of magnetic power P_h , the loss of electrical power P_{CU} , and the loss of mechanical power P_f

$$H_m = P_h + P_{CU} + P_f \quad (13)$$

In Equation (14), the magnetic loss P_h contains the hysteresis loss P_t and the eddy current loss P_E , which is calculated by:

$$P_h = P_t + P_E \quad (14)$$

With

$$P_t = C f B_{\max}^2 \quad (15)$$

$$P_E = \frac{\pi^2 t^2 (f B_{\max})^2}{6 \rho \gamma_c} \quad (16)$$

In Equations (15) and (16), C is a constant value related to electrical steel, f is the magnetization frequency, B_{\max} is the maximum magnetic flux density, t is the thickness of the silicon steel sheet, γ_c is the density, and ρ is the electrical resistivity of the iron core. In addition, the P_{CU} electrical loss can be calculated by:

$$P_{CU} = \frac{I^2 \rho_c L}{S} \quad (17)$$

where I is the intensity of the electric current and ρ_c , L and S are respectively the resistivity, length, and area of the conductor.

Finally, the calculation of the mechanical loss P_f will be:

$$P_f = \pi C' \rho_{ar} \omega^3 R_f^4 L_f \quad (18)$$

where C' is the coefficient of friction, R_f is the outer radius, L_f is the length of the rotor, ω is the angular speed of the rotor, and ρ_{ar} is the density of air [20].

3.1.5. Heat Generation by the Axis Motors

They generate heat mainly due to the conversion of electrical energy into mechanical motion. This conversion process is not perfectly efficient, and a portion of the energy is dissipated as heat. To evaluate and manage the heat generated in the axis motors of machine tools, it is important to precisely characterize this phenomenon. To mitigate the effects of heat in the axis motors of machine tools, various heat management strategies can be implemented. The heat generated by motors in MT is a very complex process. The generation of heat (H) in the motor is calculated by the following equation:

$$H = (1 - \eta) \frac{M_T * n}{9550} \quad (19)$$

where is H the motor output torque, n is the motor rotational speed and η is the motor efficiency M_T [17].

3.2. Numerical Model Formulation

The MT model is built so that FEM modeling is prepared based on the following assumptions: 1) The machine structure is considered as elastic, homogeneous, and isotropic materials. 2) Frictional losses can be neglected, as they are of less importance compared to other heat sources. 3) Small size elements in the MT structure, such as nuts, holes, etc., are omitted. 4) Thermal radiation is not considered. **Figure 1** presents an illustration of the MT structure design and the mesh model as produced using FEM. The 3D model is built using a very well-known commercial software. The mesh model is structured in 447,680 elements (with 105,639 mesh points) using shapes tetrahedral and triangular for adequate accuracies.

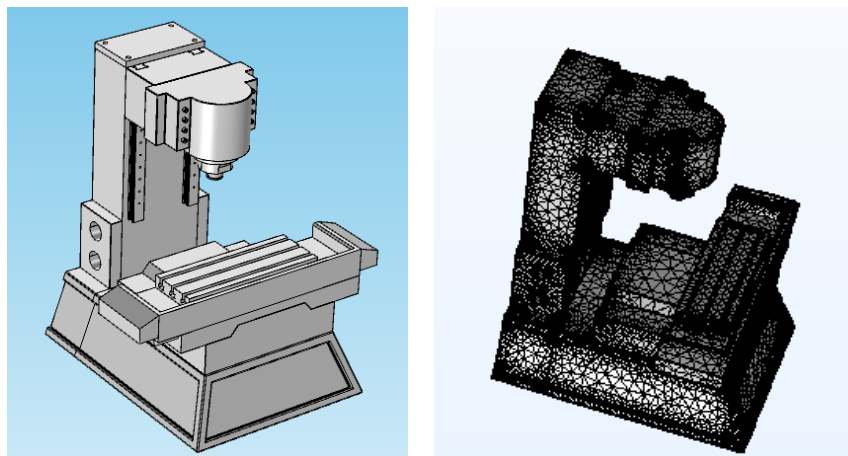


Figure 1. Finite element method model of the MT: CAD model and mesh model.

3.3. Modelling Condition and Preliminary Results

The heat sources are previously characterized experimentally using data obtained from a thermal imaging camera to calibrate the model with the appropriate boundary conditions. A FLIR A325 thermal imaging camera is used to record a sequence of thermal images of temperature distributions across the MT structure. This camera provides a sensitivity of 0.08°C , and an absolute accuracy of $\pm 2\%$. The thermal imaging camera offers a continuous picture of the temperature distribution and provides heat distribution during heating and cooling cycles. The thermal images are saved as a matrix of temperatures and analyzed using a dedicated Matlab functions to extract the temperature data by averaging groups of pixels at specific points.

The produced data associated to the desirable thermal analysis modes are as briefly defined using the following operating condition cycles:

- 1) Time-varying environmental temperature.
- 2) Temperature variation induced by heat sources in feed driving axes in X , Y , and Z directions.
- 3) Temperature variation induced by spindle rotational speed.

3.3.1. Environmental Temperature Variation

The environmental temperature variation may lead to the increase of thermally induced errors. For this purpose, the environmental temperature is collected for 8 h without axis displacement and without spindle rotation. The results presented in **Figure 2** show that the environmental temperature effect is very small (less than $1\ \mu\text{m}$) and no clear correlation between temperature and thermal error can be established (less than 1%). This is due to the irregularity of thermal error growth at a normal range of temperature. Thus, the contribution of the environmental temperature to thermal error variation can be neglected.

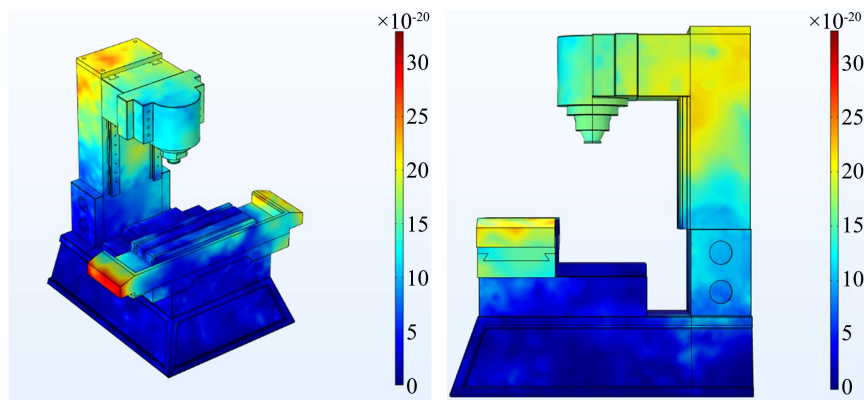


Figure 2. MT deformation estimated by the model under environment temperature.

3.3.2. Temperature Variation Induced by Displacement in X , Y , and Z Directions

Temperature variation induced by heat sources in feed driving axes X , Y , and Z directions include three-axis drive motor power loss, slider rail friction heat, friction heat of the lead screw nut, electrical components, tool-drive motor heating. The three-axis drive affects the temperature distribution of the machine bed, workbench and column, causing thermal deformation of the whole machine and thus degrading the mechanical machining accuracy. The moving range of a feed driving axis is small and intermittent compared to that of the spindle. The movement cycle is defined with speed of 15 m/min. Only the temperatures of the ball screw nut and shaft, linear guide rail and carriage are measured during the experiment. The preliminary stage successfully permitted specifying and characterizing the thermal behavior of ball screw and linear guide of the three-axis feed driving systems. The results presented in **Figure 3** and **Figure 4** show a great concordance between the heated and displacement zones. The temperature varies between 20°C and 27°C and the heat sources in feed driving axes has a relatively moderate but not negligible effect on the MT accuracy (2 to $4.5\ \mu\text{m}$).

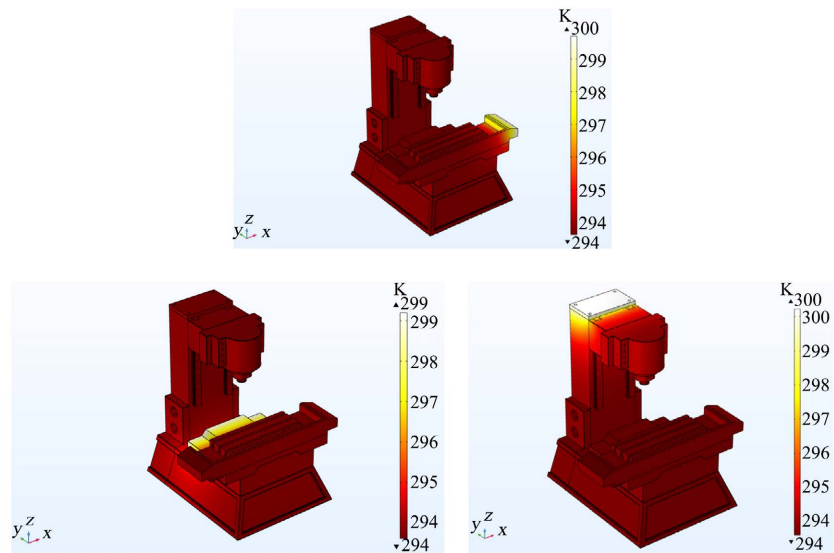


Figure 3. Temperature fields estimated by the model under heat sources in X , Y , and Z axis.

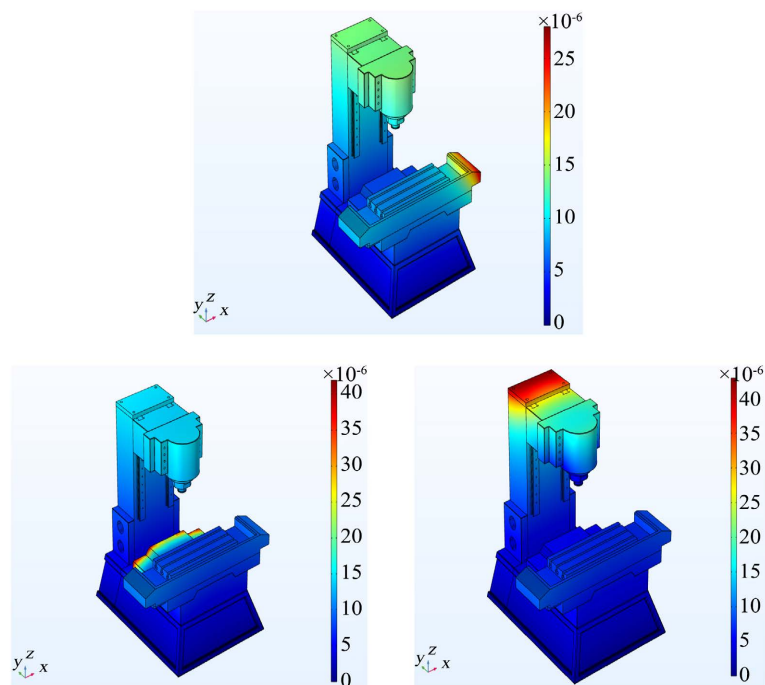


Figure 4. Estimated deformation by the model under heat sources in X , Y , and Z axis.

3.3.3. Temperature Variation Induced by Spindle Rotational Speed

Preliminary experimental investigation results indicate a powerful connection between thermal errors and medium temperature growth by the spindle axis, which is strongly correlated to the spindle speed. As rotating speed of spindle may randomly change in actual machining process, the experiment is carried out using various rotating speeds to assess this correlation. The temperatures and thermal errors variation are evaluated at the spindle speed of 600, 1200, 2400,

and 3600 rpm, respectively. In each test, the spindle rotates at a preset rotating speed for 4 h and then remains stopped for 4 h. The obtained results are shown in **Figure 5**. The results reveal that the thermal drifts and the average temperature profiles does not increase proportionally with the speeds. However, it should be noted that the thermal drifts growth corresponds well with the temperature variations. This particularity presents a real advantage in the predictive modeling process. The results presented in **Figure 5** show that the temperature varies between 20°C and 30°C and the effect of heat induced by the spindle systems can reach 50 μm. **Figure 6** and **Figure 7** present temperature fields and deformation estimated by the model under heat sources induced by the spindle and the X, Y, Z axis systems simultaneously. It can be observed that the temperature varies between 20°C and 32°C and the combined effect of heat induced by the three axe and the spindle systems can reach 70 μm.

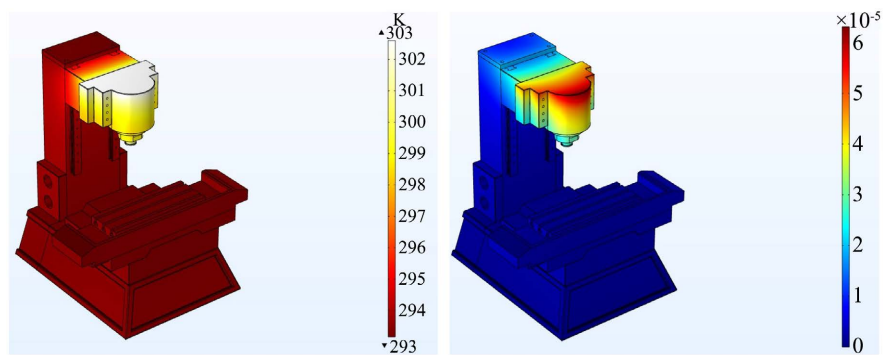


Figure 5. Temperature fields and deformation estimated by the model under heat sources induced by the spindle.

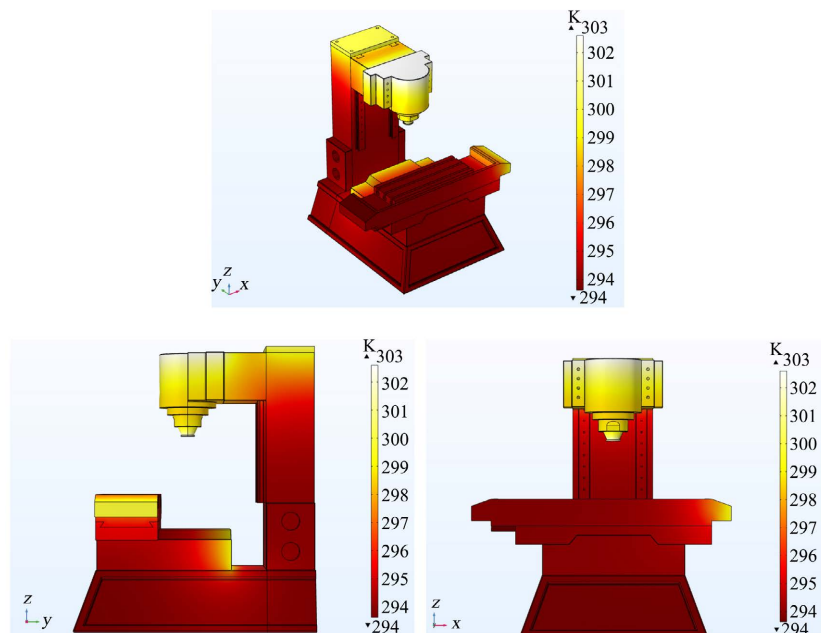


Figure 6. Temperature fields estimated by the model under heat generated by the spindle and X, Y, Z axis.

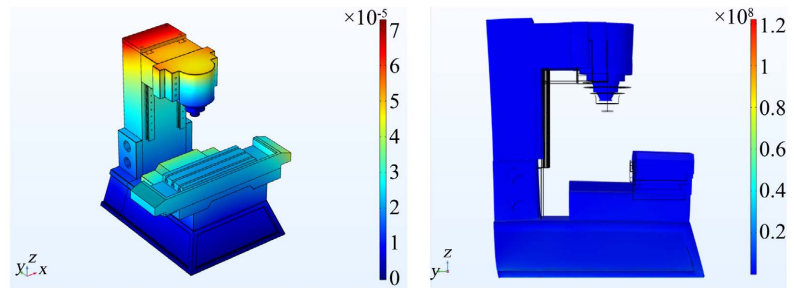


Figure 7. Estimated deformation under heat generated by the spindle and X , Y , Z axis.

4. Numerical Model Validation

The validation process of the established model aims to compare the thermal displacements estimated by the FEM based model with those of the experimental results. The experimental measurements required specialized devices in order to evaluate the temperature increase in different positions of the MT structure and the thermal deformation represented by the positioning errors of the spindle and along the three axes.

Figure 8 presents specific illustration of the used devices for temperature and induced thermal errors: 1) 16 thermistors with measuring range from -20°C to 120°C and resolution of 0.0625°C to monitor the temperature distribution in the most sensitive parts of the MT, 2) the positioning error in X , Y and Z directions, according to the ISO230-2 standard, using an API XD laser interferometer system and 3) the spindle thermal drifts, according to the ISO230-3 standard [25] [26] using the five displacement non-contact sensors method. Temperatures and thermal errors must be measured simultaneously so that each set of thermal error corresponds to a specific temperature distribution. Four sets of data are produced to test the 3D numerical model, three for the axes and the fourth for the spindle.

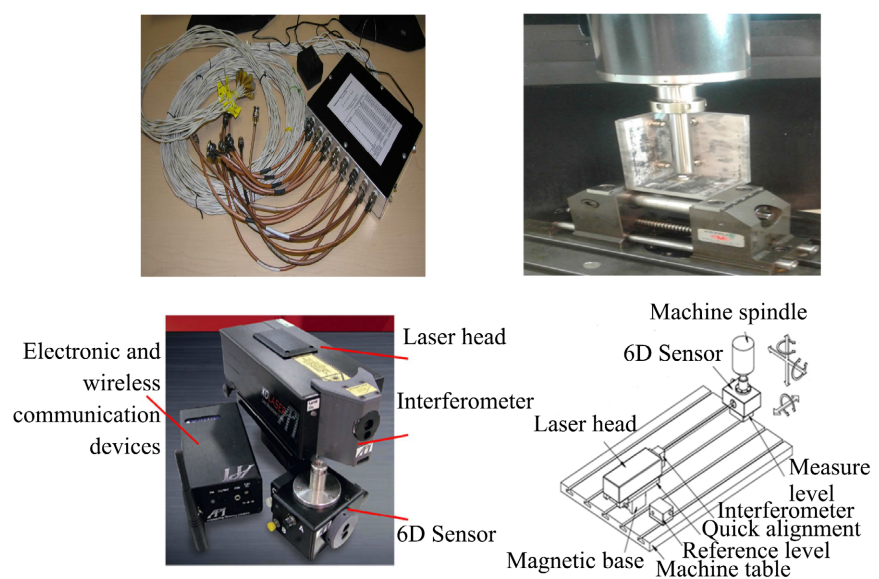


Figure 8. Temperature and thermal error measurement.

As illustrated in **Figure 9**, the adopted validation procedure for the three axes consists of comparing the measured and estimated thermal error at 9 carefully selected points, 3 points along each axis: (A B C) in X direction, (I J K) in Y direction, and (P Q R) in Z direction. The validation of the model for the spindle represents a standard case. It will not be presented in this paper.

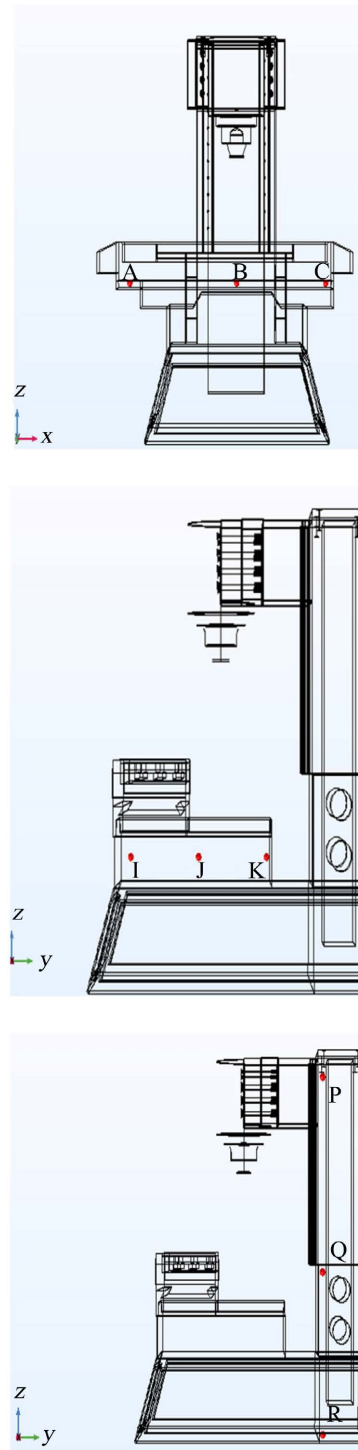


Figure 9. Localisation of the selected validation points along the X , Y , and Z axis.

Figure 10 shows the graph of the comparative evolution of the thermal behavior during the experimental measurements and the numerical analysis during a 4-hour operation with 15 m/min as constant speed for the three linear axes and 1200 rpm as rotation speed for the spindle. This comparison concern points B, J and Q. These points represent the midpoint of the travels on the X , Y and Z axes. Note that the measured temperature increased quicker than the temperature obtained through the simulation. This is due to the need to adjust the forced convection thermal boundary condition. However, the temperatures reached practically the same final temperature. The largest errors occurred at the beginning of the heating cycle since the thermal stabilization in the simulation occurred more slowly. In the first 60 min, the prediction error reached approximately 10%.

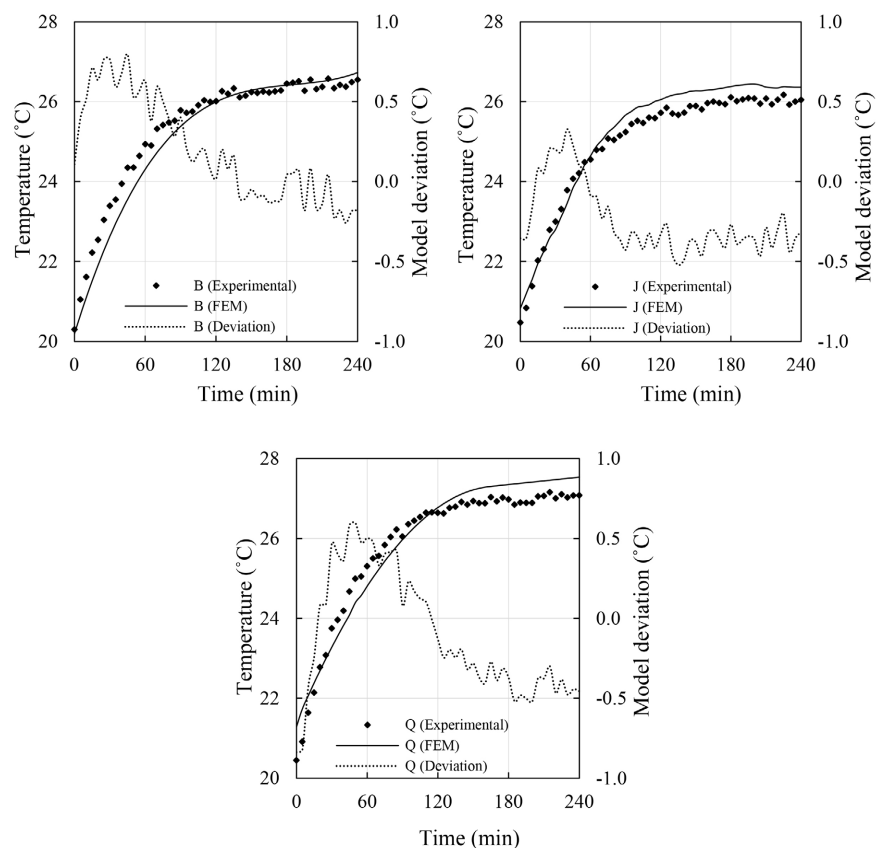


Figure 10. Comparison of the thermal behavior of the linear guide: temperature predicted by FEM analysis versus experimental temperature measurement.

Figures 11-13 show the experimental and simulated results for X , Y and Z axes respectively. For each axis, the simulation and measurement were carried out while the other two axes were in idle mode. The observed thermal error in Z -axis direction is higher than in the other directions. The largest differences are recorded at points C, K and R. These are the points that are very close to the heat sources (**Table 1**).

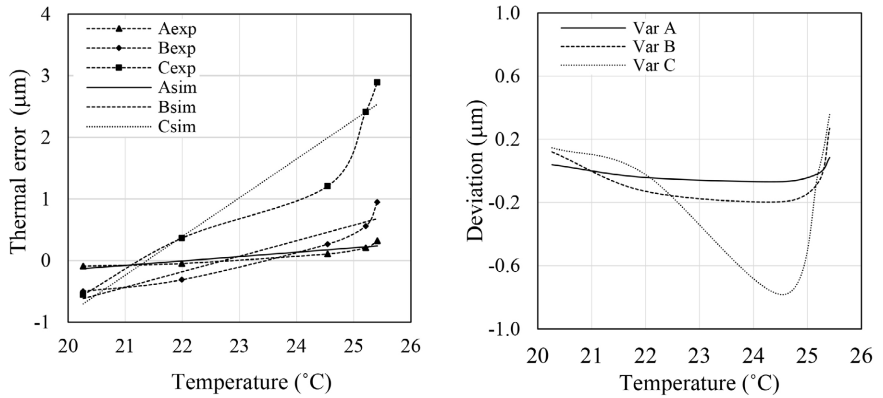


Figure 11. Predicted vs measured errors in X direction.

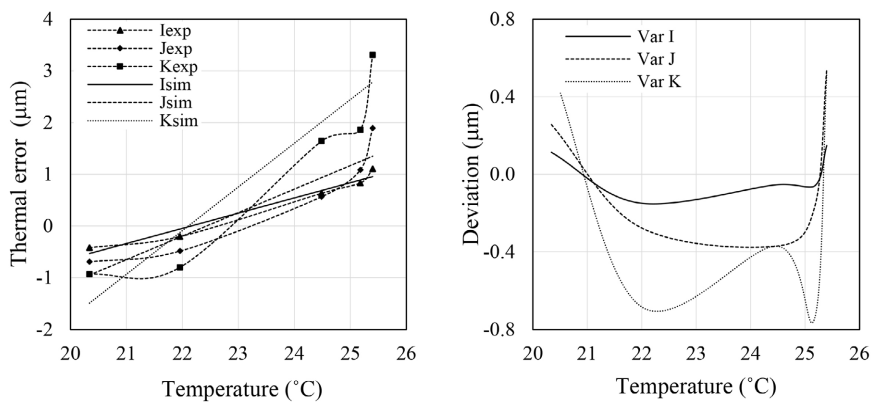


Figure 12. Predicted vs measured errors in Y direction.

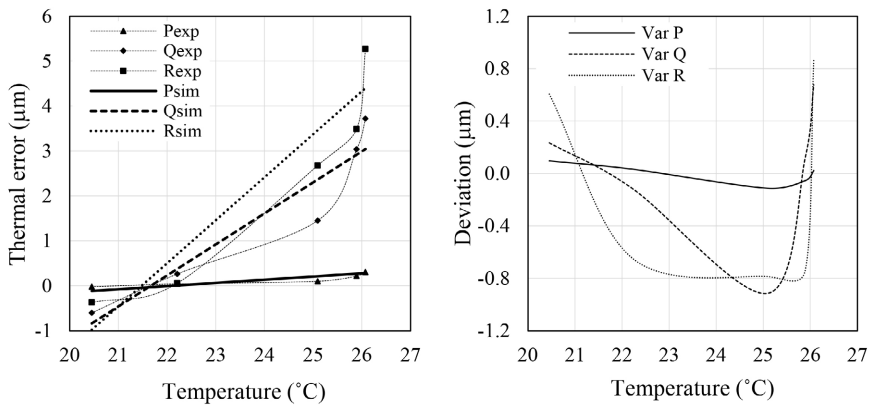


Figure 13. Predicted vs measured errors in Z direction.

Table 1. Differences between measured and estimated thermal error in the selected testing points along the X, Y, and Z axis.

Average Temperature (°C)	Numerical model deviation in testing points along the X, Y, and Z axis (µm)								
	Var A	Var B	Var C	Var I	Var J	Var K	Var P	Var Q	Var R
20.26	0.04	0.12	0.15	0.11	0.26	0.56	0.10	0.23	0.61

Continued

22.05	-0.04	-0.13	-0.02	-0.15	-0.27	-0.68	0.03	-0.11	-0.64
24.70	-0.07	-0.19	-0.78	-0.05	-0.37	-0.37	-0.11	-0.91	-0.79
25.43	-0.01	-0.07	0.00	-0.06	-0.16	-0.74	-0.05	0.12	-0.74
25.85	0.08	0.27	0.36	0.15	0.54	0.52	0.02	0.68	0.87

The position variation estimated by the FEM model at point C in the *X*-axis direction reached 2.54 μm whereas the experimentally measured value was 2.89 μm , with an error of 12.32%. The estimated value reached at point K in the *Y*-axis direction was 2.80 μm , whereas the value experimentally obtained was 3.31 μm with an error of 15.40%. At the point R in the *Z*-axis direction, the estimated error was 4.40 μm during simulation and the measured error 5.27 μm during test cycle, reaching an error of 16.50%.

The percentage errors determined between the results from the numerical simulations with the experimental results may give the impression of a high error and that the model is not good enough. However, it should be noted that the reported data only concern exclusive simulations in order to estimate thermal errors at specific locations for a small period. When the numerical modeling is used to estimate thermal errors as a function of time over a 2 to 4 hours period, the thermal errors long the three axes vary between 26 and 39 μm with estimating percentage error between 5% and 10%. It should be noted also that the relative error calculated between numerical simulations and experimental data do not exceed 5 μm in the worst case.

5. Simulation and Identification and Location of the Sensors

After validating the capacity of the numerical model to correctly estimate the temperature distribution and the resulting thermal distortions, a series of FEM numerical simulations was conducted to carry out an integrated transient thermomechanical analysis of the entire machine center under several constant, progressive, and random MT operating conditions. The results of these simulations will make it possible to fractionate the temperature field into a plurality of regions according to the estimated temperature field and to evaluate the correlation intensity index between temperatures and thermal errors in these regions, to identify in a structured way, the number and the best location for the temperature measurement sensors.

Six different 4-h operation cycles are carried out in the MT to explore the indicators and parameters that can describe the relationships between thermal errors and temperature gradients and total thermal error, totaling 24 h of tests. Due to the long-time span demanded, the tests are not replicated. The *X*, *Y*, and *Z* axes are repetitively moved at two different speeds, simulating typical MT operation in industry. The spindle rotation speed is set according to three operating cycles using constant speed, progressive speed and random speed.

The results collected during the different simulations, both in terms of temperature distribution and correlation between temperature and thermal errors suggest promoting the following recommendations.

- Place the sensors to reflect the midpoints of the identified thermal regions.
- With the highest correlation between temperatures and thermal errors.
- Select a reference point preferably in a cold zone.
- Place sensors as close to the heat sources as possible.
- Select positions to reflect temperature gradients in the three directions.
- Consider positions to reflect the temperature variation along each axis.
- Distribute uniformly the selected positions throughout the entire MT.
- Consider positions to respect a certain symmetry in the distribution of sensors.
- Eliminate redundancies and reduce the number of the selected locations.

Considering these recommendations, it clearly appears that only 11 sensors would be sufficient to experimentally describe the thermal behavior of the MT and can offer an accurate and reliable thermal mapping of both in terms of temperature and in terms of thermal errors. The locations of temperature sensitive points are illustrated in **Figure 14** and explicitly listed in **Table 2**.

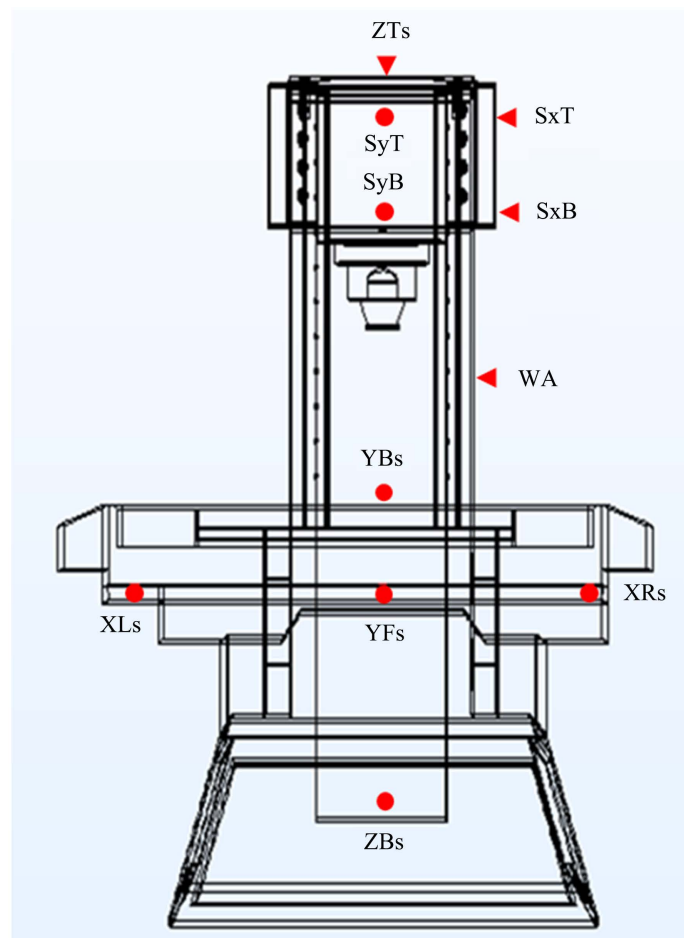
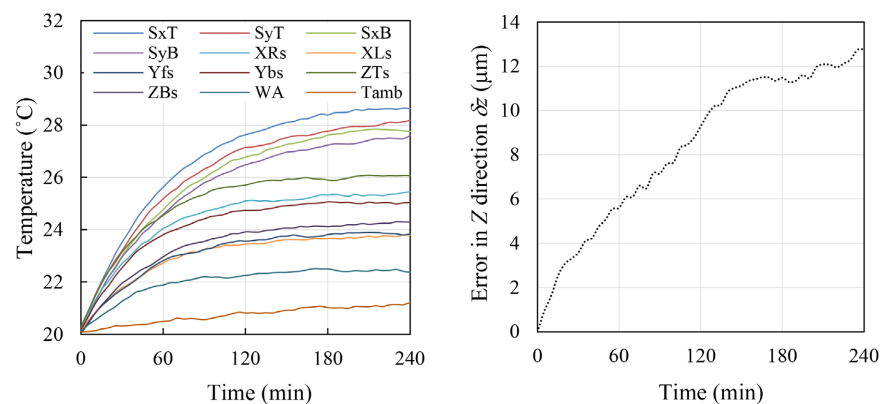


Figure 14. Temperature sensor locations.

Table 2. Identification of the specific locations of the selected temperature sensitive points.

Sensors	Location
SxT	Spindle Top side in X direction
SyT	Spindle Top side in Y direction
SxB	Spindle Bottom side in X direction
SyB	Spindle Bottom side in Y direction
XR _s	The motor on the X -axis/Right side
XL _s	Support based on the X -axis/Left side
YB _s	Support based on the Y -axis/Back side
YF _s	The motor on the Y -axis/Front side
ZT _s	The upper region of the column/Top side
ZB _s	The lower region of the column/Bottom side
WA	MT Working area

To evaluate the efficiency of the selected temperature sensitive points, a series of experimental tests is conducted to produce a database allowing the establishment of an accurate and robust thermal error predictive model. To illustrate the proposed evaluation approach, the spindle displacement in the Z direction (δz) modelling is given as an example in this paper. For this purpose, the experimental setup is adapted to consider the new 11 positions of the temperature sensors. Four spindle thermal error experiments are planned at spindle speed of 600, 1200, 2400, and 3600 rpm. The machine tool was run for 4 h at each programmed rotating speed and stopped for another 20 h. Online data of the spindle displacement are sampled at a frequency of 20 sec. An example of the measurement results at spindle speed of 1200 rpm is presented in **Figure 15**. Overall, for the 4 experiments, the average temperature varied between 25°C and 28°C and reached a maximum of 34°C around the spindle. The maximum displacement in the Z direction varied between 12 and 22 μm .

**Figure 15.** Typical measured temperature and spindle thermal errors at 1200 rpm.

While various modelling techniques can be used to build the thermal error predictive model, a multilayer feed-forward neural network seems to be one of the most appropriate options because of its simplicity and flexibility [27] [28]. The network inputs are the temperature measured at the 11 selected sensitive points (Figure 14 and Table 2) and the output are the thermal errors. The produced experimental data is randomly divided into two groups used for training (75%) and validation (25%) of the spindle thermal errors predictive model. The performance of the produced model is evaluated using five improved statistical criteria such as: Mean absolute deviation (MAD), Mean absolute percentage error (MAPE), Root mean square error (RMSE), determination coefficient (R^2), Predicted residual error sum of squares (PRESS). The measured and predicted δz , are shown in Figure 16. The statistical indicators of the model performance are summarized in Table 3.

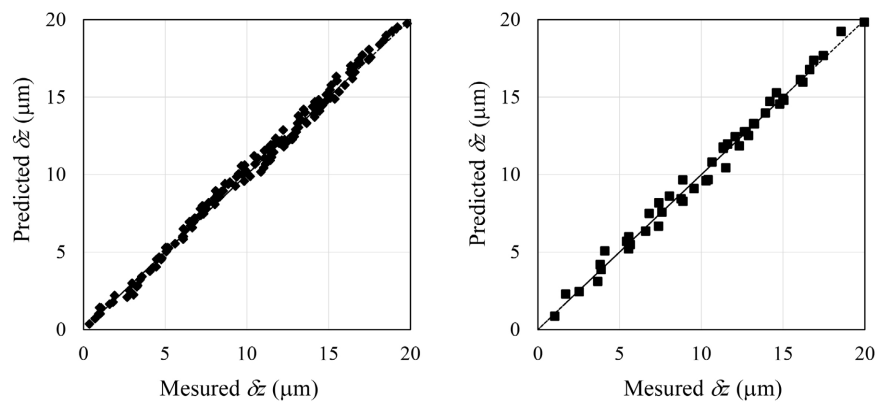


Figure 16. Measured and predicted spindle thermal errors in training and validation phases.

Table 3. Evaluation results of the predictive model.

	MAD	MAPE	RMSE	R^2	PRESS
Training	0.1995	3.36%	0.0178	99.83%	0.0584
Validation	0.3038	6.78%	0.0380	99.03%	0.1970

These results suggest that the selected key temperature points are appropriate to describe MT thermal state and the modeling approach can be effective for an efficient error compensation process. Experiments covering more spindle speed for more training and validation data as well as an improvement of the modeling procedure can lead to more accurate and efficient models. This may probably lead to an improved predictive model decreasing the modelling error to less than 5%.

6. Conclusion

The present paper introduces a numerical investigation of thermal behavior of CNC MT and its effects on dimensional accuracy of machined parts. The inves-

tigations are based on exhaustive modelling and simulation efforts carried out using a 3D finite element thermomechanical analysis and structured experimental study. The temperature distribution and the thermally induced error characteristics are used to evaluate the effects of heating source intensity, thermal distortion of MT component, and their interactions on dimensional accuracy of machined parts. A structured experimental design combined with improved statistical analysis tools are used to assess the 3D model performance. The experiments are performed on a vertical machining center using temperature sensors, thermal imaging, laser interferometer and displacement non-contact sensors. Extensive simulations carried out reveal that the developed 3D numerical model can estimate the temperature distribution in the MT accurately with a maximum error of less than 10%. The model accuracy is confirmed by coefficients of determination greater than 95%. The maximum error is observed at the beginning of the heating cycle since the thermal stabilization in the simulation occurred more slowly. When the numerical model is used to estimate thermal errors as a function of temperature and time over a 2 to 4 hours period, the thermal errors along the three axes vary between 26 and 39 μm with estimated percentage error between 5% and 10%. Globally, the modelling and validation results indicate that the proposed numerical model can lead to consistent and accurate estimation of temperature distribution and thermal distortions. The proposed model also provides an appropriate basis to carry out a unified transient thermomechanical analysis of the entire machine center under several constant, progressive, and random MT operating conditions. The results of these simulations allowed us to divide the temperature field into several regions according to the local estimated temperature and to evaluate the correlation intensity index between temperatures and thermal errors in these regions. These actions made it possible to identify in a structured way, the number, and the best location for the temperature measurement sensors. To evaluate the efficiency of the proposed temperature sensitive points, a series of experiences is conducted to produce the data needed to develop an empirical model for predicting the thermal errors as function of MT thermal state and examine if the selected key measurement points are appropriate. The case of the spindle displacement in the Z direction (δz) is given as an example to illustrate this verification. With the encouraging results obtained using this model, the ANN based real time prediction and compensation will be the subject of additional investigations to generate more numerical simulations and experimentations to develop more accurate, robust and cost-effective predictive modelling approach.

Conflicts of Interest

The authors declare no conflicts of interest regarding the publication of this paper.

References

- [1] Bryan, J. (1990) International Status of Thermal Error Research (1990). *CIRP An-*

- nals*, **39**, 645-656. [https://doi.org/10.1016/s0007-8506\(07\)63001-7](https://doi.org/10.1016/s0007-8506(07)63001-7)
- [2] Tan, B., Mao, X., Liu, H., Li, B., He, S., Peng, F., et al. (2014) A Thermal Error Model for Large Machine Tools That Considers Environmental Thermal Hysteresis Effects. *International Journal of Machine Tools and Manufacture*, **82**, 11-20. <https://doi.org/10.1016/j.ijmactools.2014.03.002>
- [3] Ramesh, R., Mannan, M.A. and Poo, A.N. (2000) Error Compensation in Machine Tools—A Review. *International Journal of Machine Tools and Manufacture*, **40**, 1235-1256. [https://doi.org/10.1016/s0890-6955\(00\)00009-2](https://doi.org/10.1016/s0890-6955(00)00009-2)
- [4] Ramesh, R., Mannan, M.A. and Poo, A.N. (2000) Error Compensation in Machine Tools—A Review. *International Journal of Machine Tools and Manufacture*, **40**, 1257-1284. [https://doi.org/10.1016/s0890-6955\(00\)00010-9](https://doi.org/10.1016/s0890-6955(00)00010-9)
- [5] Li, J.W., Zhang, W.J., Yang, G.S., Tu, S.D. and Chen, X.B. (2008) Thermal-Error Modeling for Complex Physical Systems: The-State-of-Arts Review. *The International Journal of Advanced Manufacturing Technology*, **42**, 168-179. <https://doi.org/10.1007/s00170-008-1570-x>
- [6] Li, Y., Zhao, W., Lan, S., Ni, J., Wu, W. and Lu, B. (2015) A Review on Spindle Thermal Error Compensation in Machine Tools. *International Journal of Machine Tools and Manufacture*, **95**, 20-38. <https://doi.org/10.1016/j.ijmactools.2015.04.008>
- [7] Li, Y., Dai, Y., Gao, Y., Tao, X. and Wang, G. (2022) Review on Thermal Error Suppression and Modeling Compensation Methods of High-Speed Motorized Spindle. *Recent Patents on Engineering*, **17**, Article ID: e080622205713. <https://doi.org/10.2174/1872212117666220608110451>
- [8] Kim, S.K. and Cho, D.W. (1997) Real-Time Estimation of Temperature Distribution in a Ball-Screw System. *International Journal of Machine Tools and Manufacture*, **37**, 451-464. [https://doi.org/10.1016/s0890-6955\(96\)00036-3](https://doi.org/10.1016/s0890-6955(96)00036-3)
- [9] Kim, K. and Chung, S. (2004) Synthesis of the 3D Artefact for Quick Identification of Thermal Errors in Machine Tools. *International Journal of Production Research*, **42**, 1167-1187. <https://doi.org/10.1080/00207540310001614123>
- [10] Veldhuis, S.C. and Elbestawi, M.A. (1995) A Strategy for the Compensation of Errors in Five-Axis Machining. *CIRP Annals*, **44**, 373-377. [https://doi.org/10.1016/s0007-8506\(07\)62345-2](https://doi.org/10.1016/s0007-8506(07)62345-2)
- [11] Abdulshahed, A.M., Longstaff, A.P., Fletcher, S. and Myers, A. (2015) Thermal Error Modelling of Machine Tools Based on ANFIS with Fuzzy C-Means Clustering Using a Thermal Imaging Camera. *Applied Mathematical Modelling*, **39**, 1837-1852. <https://doi.org/10.1016/j.apm.2014.10.016>
- [12] Abdulshahed, A.M., Longstaff, A.P., Fletcher, S. and Potdar, A. (2016) Thermal Error Modelling of a Gantry-Type 5-Axis Machine Tool Using a Grey Neural Network Model. *Journal of Manufacturing Systems*, **41**, 130-142. <https://doi.org/10.1016/j.jmsy.2016.08.006>
- [13] Gomez-Acedo, E., Olarra, A. and Lopez de la Calle, L.N. (2012) A Method for Thermal Characterization and Modeling of Large Gantry-Type Machine Tools. *The International Journal of Advanced Manufacturing Technology*, **62**, 875-886. <https://doi.org/10.1007/s00170-011-3879-0>
- [14] Weck, M., McKeown, P., Bonse, R. and Herbst, U. (1995) Reduction and Compensation of Thermal Errors in Machine Tools. *CIRP Annals*, **44**, 589-598. [https://doi.org/10.1016/s0007-8506\(07\)60506-x](https://doi.org/10.1016/s0007-8506(07)60506-x)
- [15] Holman, J. (2010) Heat Transfer. Tenth Edition, The McGraw-Hill Companies.
- [16] Haitao, Z., Jianguo, Y. and Jinhua, S. (2007) Simulation of Thermal Behavior of a CNC Machine Tool Spindle. *International Journal of Machine Tools and Manufac-*

- ture, **47**, 1003-1010. <https://doi.org/10.1016/j.ijmachtools.2006.06.018>
- [17] Mao, X., Mao, K., Wang, F., Yan, B. and Lei, S. (2018) A Convective Heat Transfer Coefficient Algorithm for Thermal Analysis of Machine Tools Considering a Temperature Change. *The International Journal of Advanced Manufacturing Technology*, **99**, 1877-1889. <https://doi.org/10.1007/s00170-018-2605-6>
- [18] Harris, T.A. (2001) Rolling Bearing Analysis. Wiley.
- [19] Takabi, J. and Khonsari, M.M. (2013) Experimental Testing and Thermal Analysis of Ball Bearings. *Tribology International*, **60**, 93-103. <https://doi.org/10.1016/j.triboint.2012.10.009>
- [20] dos Santos, M.O., Batalha, G.F., Bordinassi, E.C. and Miori, G.F. (2018) Numerical and Experimental Modeling of Thermal Errors in a Five-Axis CNC Machining Center. *The International Journal of Advanced Manufacturing Technology*, **96**, 2619-2642. <https://doi.org/10.1007/s00170-018-1595-8>
- [21] Xu, Z.Z., Liu, X.J., Kim, H.K., Shin, J.H. and Lyu, S.K. (2011) Thermal Error Forecast and Performance Evaluation for an Air-Cooling Ball Screw System. *International Journal of Machine Tools and Manufacture*, **51**, 605-611. <https://doi.org/10.1016/j.ijmachtools.2011.04.001>
- [22] Verl, A. and Frey, S. (2010) Correlation between Feed Velocity and Preloading in Ball Screw Drives. *CIRP Annals*, **59**, 429-432. <https://doi.org/10.1016/j.cirp.2010.03.136>
- [23] Jang, S., Khim, G. and Park, C. (2016) Estimation of Friction Heat in a Linear Motion Bearing Using Box-Behnken Design. *The International Journal of Advanced Manufacturing Technology*, **89**, 2021-2029. <https://doi.org/10.1007/s00170-016-9165-4>
- [24] Cheng, D., Yang, W., Park, J., Park, T., Kim, S., Kim, G., et al. (2014) Friction Experiment of Linear Motion Roller Guide THK Srg25. *International Journal of Precision Engineering and Manufacturing*, **15**, 545-551. <https://doi.org/10.1007/s12541-014-0369-y>
- [25] International Standards Organization (2006) Test Code for Machine Tools—Part 2: Determination of Accuracy and Repeatability of Positioning Numerically Controlled Axes.
- [26] International Standards Organization (2007) Test Code for Machine Tools—Part 3: Determination of Thermal Effects.
- [27] Huang, S.H. and Zhang, H.-C. (1994) Artificial Neural Networks in Manufacturing: Concepts, Applications, and Perspectives. *IEEE Transactions on Components, Packaging, and Manufacturing Technology: Part A*, **17**, 212-228. <https://doi.org/10.1109/95.296402>
- [28] Meireles, M.R.G., Almeida, P.E.M. and Simoes, M.G. (2003) A Comprehensive Review for Industrial Applicability of Artificial Neural Networks. *IEEE Transactions on Industrial Electronics*, **50**, 585-601. <https://doi.org/10.1109/tie.2003.812470>